

# Formation Dynamics and Evaporative Cooling of a Dark Exciton Condensate

Subhradeep Misra<sup>1</sup>, Michael Stern<sup>2</sup>, Vladimir Umansky<sup>1</sup> and Israel Bar-Joseph<sup>1</sup>

<sup>1</sup>*Department of Condensed Matter physics, Weizmann Institute of Science, Rehovot, Israel*

<sup>2</sup>*Department of Physics, Bar-Ilan University, Ramat-Gan, Israel*

## Abstract

*We study the formation of an exciton condensate in GaAs coupled quantum wells at low temperatures. We show that the condensate consists of dark excitons, and extends over hundreds of  $\mu\text{m}$ , limited only by the boundaries of the mesa. We find that the condensate density is determined by spin flipping collisions among the condensate excitons and with the thermal bath. We show that these processes, which convert dark excitons to bright, evaporatively cool the system to temperatures that are much lower than the bath temperature. We present a rate equations model, which explains the temperature and power dependence of the exciton density, and in particular - the large density buildup at low temperatures. We confirm the validity of the model by reproducing the unique behavior observed when a magnetic field is applied in a direction parallel to the layers.*

In the dilute limit, excitons can be considered as a Bose gas, and are thus expected to undergo a Bose Einstein condensation (BEC) transition at low temperatures [1, 2]. Over the past few decades there have been many attempts to realize such a condensate in various material systems. A particularly interesting research direction, which attracted considerable attention, is using indirect excitons (IX) in coupled quantum wells (CQW) [3 - 6]. An attractive feature of this system is its long lifetime, which allows achieving the critical condensation density at moderate excitation powers, and establishing quasi-equilibrium at low temperatures. Indeed, a bulk of experimental works on CQW reported anomalous behavior that is consistent with an exciton BEC transition at low temperatures [7-16].

An important development in the quest for the exciton BEC was introduced a little over a decade ago by Combescot *et al.* [17, 18], who argued that the condensate should be dark. Their argument was based on the fact that electron-hole exchange removes the degeneracy between the bright ( $J_z = \pm 1$ ) and dark ( $J_z = \pm 2$ ) exciton energies, such that the dark exciton is lower in energy than the bright one, and hence, it should be the ground state for condensation. Indeed, a series of studies performed in the last decade provided evidence for the formation of a dark condensate [9, 11, 12, 13, 15], with the most compelling one coming from measurement of the blueshift of the IX peak energy as the temperature is decreased at constant illumination power [12]. This blueshift,  $\Delta E$ , is due to the dipole-dipole repulsive interaction among excitons and is proportional to their density [19]. Hence, its increase at low temperatures can be interpreted as a signature of a ground state occupation buildup by long-lived dark excitons.

The unique composition of the system, of short-lived bright excitons, which can recombine radiatively, and long-lived dark excitons, which can only do that through slow nonradiative processes, poses a challenge in understanding the condensate formation and the mechanisms determining its density [20]. In this work we address this challenge by studying the low temperature behavior of IX in GaAs CQW. We present conclusive evidence that a dark condensate is formed and extends over hundreds of  $\mu\text{m}$ , well beyond the excitation spot. We show that the condensate density is determined by the rate of spin flipping collisions among the condensate excitons and with the thermal bath. We find that these processes, which convert dark excitons to bright, evaporatively cool the system to temperatures that are much lower than the bath temperature. We present a rate equations model, which accounts for these interactions

and explains the temperature and power dependence of the IX blueshift, and in particular - the peculiar behavior observed when a magnetic field is applied in a direction parallel to the layers.

We begin with presenting several measurements that provide conclusive evidences for the formation of dark condensate at low temperatures. Figure 1a shows the blueshift of the IX peak energy as a function of position along a horizontal cross-section of the mesa,  $\Delta E(x)$ , normalized by its value at the center of the excitation beam. Since  $\Delta E$  is proportional to the exciton density, this measurement yields the density distribution. It is seen that at high temperatures  $\Delta E(x)$  follows approximately the illumination beam profile, which is marked by the solid red line (the small increase in the distribution width is due to diffusion [21]). Remarkably, however, as the temperature is lowered below  $\sim 6\text{K}$ ,  $\Delta E(x)$  becomes *constant* across the  $200\mu\text{m}$  wide mesa, while the PL intensity,  $I(x)$ , continues to follow the illumination beam profile. The lack of correlation between  $I(x)$  and  $\Delta E(x)$  implies that long-lived particles, which contribute to  $\Delta E$  but do not emit light, diffuse uniformly throughout the large mesa [23].

Another evidence for the presence of dark excitons comes from spectral and time resolved measurements. Figure 1b shows the IX peak energy,  $E_{IX}$ , as a function of temperature at three gate voltages,  $V_g$ , while keeping the pump power fixed at  $P = 10\mu\text{W}$ . It is seen that  $E_{IX}$  shifts to high energies with decreasing temperatures, reaching  $\Delta E = 10 - 20 \text{ meV}$  at  $T < 1\text{K}$ . These large values of  $\Delta E$  imply that the exciton density,  $n$ , increases considerably at low temperatures. To determine whether this increase of  $n$  is due to accumulation of bright or dark excitons we measure the corresponding change of the radiative rate,  $\gamma_r$ . As expected, we find that  $\gamma_r$  depends primarily on  $E_{IX}$ , and becomes faster as  $E_{IX}$  increases (Fig. 1c), reflecting the increased overlap of the electron and hole wavefunctions as the external electric field is screened. We can therefore conclude that the steady-state bright exciton density *decreases* with decreasing temperature, and cannot explain the large blueshift at low temperatures.

To further confirm the presence of a high IX density we measure the absorption spectra of the narrow and wide wells. This is done by tuning the energy of the excitation laser near the direct exciton resonance of each well, and measuring the generated photocurrent as a function of laser energy. Figure 1d shows the resulting narrow well spectrum as a function of temperature. The shift of the direct exciton line to higher

energies with decreasing temperatures and the broadening of the lower energy trion line are clear manifestations of the presence of high density of electrons in this well. Measurements conducted in the wide well shows a similar temperature dependence, confirming that a high hole density builds up in the wide well too. Solving the self-consistent Schrodinger-Poisson equation, assuming equal charges in the two wells, we could reproduce the shift of the direct exciton and obtain a density of  $\sim 5 \times 10^{10} \text{ cm}^{-2}$  at the lowest temperature [23].

A similar blueshift of the IX energy with temperature was reported in an earlier work, and interpreted as indication for the onset of dark BEC [12]. It was argued that beyond condensation threshold the condensate density is limited by the slow nonradiative recombination rate,  $\gamma_{nr}$  [20]. Accordingly, the total density should grow linearly with power,  $P$ , and since  $\Delta E \sim n^{3/2}$  for a BEC [19], we should expect a superlinear dependence of  $\Delta E$  on power,  $\Delta E(P) \sim P^{3/2}$ . However, this is not observed experimentally: Figure 2a shows the measured  $\Delta E(P)$  at several temperatures ( $V_g = -3.7V$ ). It is seen that rather than a superlinear dependence on power, the observed behavior is strongly *sublinear*: At high temperatures it can be approximated by  $\Delta E \sim P^{1/2}$ , and at low temperature – it exhibits a fast saturation towards a constant  $\Delta E$ . In fact, we can estimate  $\gamma_{nr}$  in our sample by measuring the value of  $\Delta E$  at very low temperatures and powers, before saturation sets in: We find that  $\Delta E = 5 \text{ meV}$  at  $T = 0.5 \text{ K}$  and  $P = 10 \text{ nW}$ , implying that  $\gamma_{nr}^{-1} \approx 0.3 \text{ ms}$ . (We show in the Supplementary Material section that the main contribution  $\gamma_{nr}$  is the tunneling of photo-carriers to the contacts, which gives rise to a photocurrent [23].) Clearly, at power levels of  $\sim 10 \mu \text{ W}$ , which are three order of magnitude higher, the model suggested in [20] yields non-realistic densities.

The sublinear behavior of  $\Delta E(P)$  implies that loss mechanisms, which are nonlinear in  $n$ , should be considered. Indeed, such nonlinear loss mechanisms due to interactions among the condensate particles and between them and the thermal bath, are known to play important role in atomic and cavity-polariton condensates [23, 25]. We note that these interactions are much stronger in our case, due to the large electric dipole associated with the IX. In the following, we present a rate equations model that incorporates these interactions, and is based on the generalized Gross-Pitaevskii formalism for incoherently pumped cavity polaritons [25], noting the unique two-

component nature of the thermal part in our system: (i) A long-lived dark exciton population with a steady-state density  $n_2$ , which can exchange particles with the condensate through fast momentum scattering, and (ii) a short-lived bright exciton population with density  $n_1$ , which can only do that through spin-flip processes.  $n_1$  and  $n_2$  exchange particle via spontaneous spin flip process at a rate  $\gamma_s$ . We show below that the fast decay of  $n_1$  through radiative recombination acts as a sink for the system, thereby limiting the steady-state condensate density,  $n_c$ , and effectively cools the system to mK temperatures.

The particles exchange between the three reservoirs,  $n_1$ ,  $n_2$  and  $n_c$ , and with the environment, is schematically depicted in Fig. 2b. The thermal bath is pumped at a rate  $P$ , and the condensate is formed through stimulated momentum scattering at a rate  $W^+ = Rn_2n_c$  [23, 25]. We argue that  $n_c$  is determined by three loss mechanisms:

- i.* The first mechanism is simply through non-radiative recombination at a rate  $\gamma_{nr}n_c$ .
- ii.* The second loss mechanism is due to collisions among the condensate excitons:  $|+2\rangle + |-2\rangle \rightarrow |+1\rangle + |-1\rangle$ , where 1, 2 are the total angular momentum  $J_z$  of the exciton. This process converts two condensate dark excitons into two bright ones through particle exchange, and results in a fast removal of excitons from the system by radiative recombination. The rate of this process can be expressed as  $\alpha n_c^2$ , where  $\alpha = \alpha_0 \exp(-\frac{U_0}{k_B T})$ . Here  $\alpha_0 = |\xi|/h$ ,  $\xi$  is the exchange integral density [20, 23], and  $U_0$  is the height of an effective hard-wall repulsive potential. Rewriting  $\alpha = \alpha_0 \exp(-\frac{T_0}{T})$  we can define a characteristic temperature,  $T_0$ , below which this scattering process is exponentially suppressed and the condensate density increases.
- iii.* Finally, interactions between the condensate and the thermal bath give rise to a third loss mechanism. The spin flip mechanism, which is dominant for thermal excitons in coupled quantum wells [26], is the Dyakonov-Perel (DP) [26]. The main contribution to it comes from the Rashba term, which converts the crystal electric field (due to non-centro symmetry of the lattice) to an effective magnetic field. In the regular case of thermal excitons, momentum scattering with impurities changes the direction of the exciton motion in the crystal, and consequently - the direction of the effective B field changes, thereby changing the exciton precession angle. The accumulation of such scattering events gives rise to loss of spin orientation in a

random walk process. The idea in our case is that for the condensate - the necessary momentum scattering is provided by collisions with the thermal excitons, and the density of impurities, which appears in the DP expression, is replaced by the density of the thermal excitons. Accordingly, the rate of this process can be expressed as  $\beta n_1 n_c$ , and should have a much weaker (non-exponential) temperature dependence. We shall elaborate more on this mechanism when discussing the magnetic field results.

These assumptions can be formulated in three rate equations for  $n_1$ ,  $n_2$  and  $n_c$ , where the thermal bath is continuously pumped at a rate  $P$ , and the loss to the environment is through radiative and non-radiative processes [23]. Solving these equations we obtain the steady-state density of  $n_1$ ,  $n_2$ , and  $n_c$  as a function of power and temperature. The total density  $n(P, T) = n_1 + n_2 + n_c$  is depicted in Fig. 2c, where the increase of  $n$  with decreasing temperature at constant power, and the sublinear dependence of  $n$  on  $P$  are clearly seen. Remarkably, at low temperatures the density becomes approximately constant at high power, almost independent of  $P$ . In this regime the increased pumping rate is compensated by the loss due to the  $\beta n_1 n_c$  term, and the condensate density does not rise with power.

An insight to this behavior can be obtained by neglecting the slow  $\gamma_{nr}$  and  $\gamma_s$  terms [23]. With these approximation the condensate density at steady state can be expressed as

$$(1) \quad n_c \approx \frac{P\beta}{\alpha\gamma_r} \left[ \left( 1 + \frac{\alpha\gamma_r^2}{P\beta} \left[ \frac{1}{\beta} - \frac{1}{R} \right] \right)^{1/2} - 1 \right]$$

It can easily be seen that in the limit of low power and high temperatures  $n_c \sim C_1 \sqrt{P}$ , whereas at the opposite limit of high power and low temperatures – the power dependence factors out and  $n_c \sim C_2$ . (Here,  $C_1 = C_1(\alpha, \beta, R)$  and  $C_2 = C_2(\gamma_r, \beta, R)$  are functions of these parameters [23]).

The solid lines in Fig. 2a are the calculated temperature and power dependent blueshift obtained using the full solution of the model, where we used

$$(2) \quad \Delta E = 4\pi e^2 d(n_1 + n_2) f_{th} / \epsilon + 10e^2 d^2 n_c^{3/2} / \epsilon.$$

Here  $d$  is the dipole length,  $\varepsilon$  is the dielectric constant,  $f_{th}$  is the density and temperature dependent correlation factor of the thermal gas [19], and we used the expression derived in Ref. [19] for the condensate blueshift [23]. It can be seen that the model accurately captures the observed temperature and power dependence of  $\Delta E$ . In constructing the solutions depicted in Fig. 2a we used the measured values of  $\gamma_r$  (Fig. 1c) and  $\gamma_{nr}^{-1} = 0.3\text{ms}$ , and looked for best fit for the parameters  $T_0$ ,  $\alpha_0$  and  $\beta$ . We find that these three parameters affect different aspect of the behavior, and hence can be fitted almost independently:  $T_0$  determines the temperature dependence, and  $\alpha_0$  and  $\beta$  – the power dependence at high and low temperatures, respectively.

Remarkably, we find approximately the same value of  $T_0 \approx 7\text{K}$  for the three measured gate voltages,  $V_g = -2.5\text{V}$ ,  $-3.3\text{V}$ , and  $-3.7\text{V}$ . Hence, the increase  $\Delta E$  with reducing temperatures can be understood as a straightforward consequence of the exponential inhibition of the two-particle scattering process at  $T \ll T_0$ . This allows dark exciton accumulation at the condensate and consequently – clear manifestation of BEC effects. We note that  $T_0 \approx 7\text{K}$  corresponds to a hard-wall potential height of  $U_0 \approx 0.5\text{meV}$ , which is the value of the screened exciton-exciton repulsive potential at approximately  $\sim 2a_B$ , where  $a_B$  is the exciton radius [1]. When  $k_B T > U_0$  the exciton kinetic energy is sufficient to tunnel into the region  $r < 2a_B$ , and the probability for particle exchange substantially increases [20].

We find that the values for  $\alpha_0$  is  $1.5 \times 10^{-8}\text{m}^2\text{s}^{-1}$ . This value is in excellent agreement with the calculation of Ref. [20] for the exchange integral  $\xi$  using  $d = 18\text{nm}$ , which is the dipole length in our sample [23], thereby providing a strong support for the model. The crossing of the IX line with the direct exciton does not allow us to explore  $\Delta E$  at the fully saturated regime (low  $T$  and high  $P$ ). Hence, while there is some ambiguity in the exact value of  $\beta$ , we find that it is  $\sim 10^{-8}\text{m}^2\text{s}^{-1}$ , of the same order of magnitude as  $\alpha_0$ . The fitted value for the stimulated scattering  $R$  is  $1.2 \times 10^{-7}\text{m}^2\text{s}^{-1}$ , and we took it to be temperature independent.

We can use the calculated thermal density,  $n_{th} = n_1 + n_2$ , to extract the effective temperature of the system,  $T_{eff}$ . For an ideal BEC in 2D, this density is given by  $n_{th} = k_B T_{eff} M / \hbar^2$ , where  $k_B$  is the Boltzmann constant and  $M$  is the exciton mass, and hence,  $T_{eff}$  can be determined using the value of  $n_{th}$ . Figure 2d shows the calculated  $T_{eff}$  as a function of the bath temperature,  $T_{bath}$ , for pump power of 1 and  $10\mu\text{W}$  and

$V_g = -3.7V$ . Remarkably, it is seen that  $T_{eff} \ll T_{bath}$  throughout, with the difference being pronounced particularly at low temperatures: The suppression of the two particles scattering at  $T \ll T_0$  and the faster removal of bright excitons from the system due to the larger blueshift, gives rise to a reduction of  $n_{th}$ , and consequently – to evaporative cooling of the system. We should note here that this argument breaks down at low condensate densities (very low power or high temperature), where disorder plays a role and gives rise to fragmentation of the condensate. This limit will be discussed elsewhere.

To test the validity of the rate equation model we measure the behavior of the system when a magnetic field parallel to the CQW layers is applied,  $\mathbf{B}_{||} = \hat{\mathbf{x}}B$ . Under such field the exciton dispersion in the direction normal to it,  $\hat{\mathbf{y}}$ , is shifted such that its minimum is at  $k_y = eBd/\hbar$ . At  $B > 1\text{T}$  this minimum resides outside the radiative zone, e.g.  $eBd/\hbar > k_0 = E_{IX}\sqrt{\epsilon}/\hbar c$ , and only a fraction of the excitons can recombine radiatively. Hence, the effective radiative lifetime of the system is expected to grow with  $B$  [29]. Indeed, we find a 40 fold increase from 40ns to  $\approx 1.6\mu\text{s}$  as  $B$  is increased from 0 to 4T while keeping the power and temperature constant (Fig. 3a).

The growth of the radiative lifetime should give rise to a large increase of  $n_1$ , and thereby strongly modify the behavior of the system. We expect a competition between two opposing trends: An increase of  $\Delta E$  due to the buildup of the thermal exciton density, and a decrease of it due to the depletion of the condensate by the loss term  $\beta n_1 n_c$ . Figure 3b shows the calculated thermal and condensate density as the magnetic field is increased at constant temperature and power. The buildup of the thermal density and the depletion of the condensate are clearly seen. In Fig. 3c we show the corresponding calculated blueshift due to each component, and the total  $\Delta E(B)$ . It is seen that the signature of this competition is a pronounced dip in  $\Delta E(B)$  curve.

Figure 3d shows the observed  $\Delta E(B)$  for several temperatures. We can see that at  $T = 2.9\text{K}$ , where the condensate density at  $B = 0$  is relatively small, the dominant process is the buildup of the thermal exciton density, manifested as a monotonous increase of  $\Delta E$  with  $B_{||}$ . However, as the temperature is lowered and the zero-field condensate density becomes larger, we observe a dip around  $B \approx 2.5\text{T}$ , and as expected - it becomes more pronounced as the temperature is lowered [30]. The appearance of the



predicted dip can be therefore considered as confirming the importance of the interactions between the condensate and the thermal bath.

The solid lines in Fig. 3d depicts the calculated behavior using the measured values of  $\gamma_r$  and PL intensity,  $I$ , and the parameters  $\alpha_0$ ,  $T_0$ , and  $\gamma_{nr}$  are kept at their zero field value [31]. Since  $\beta$  is related to the spin flip rate  $\gamma_s$ , we vary it with magnetic field as  $\beta(B) = \beta(0)B^{-1/2}$ , consistent with the expected decrease of  $\gamma_s$  with  $B$  [32]. It is seen that we can nicely reproduce the appearance of the dip at low temperatures, and its disappearance as the temperature is increased. The excellent quantitative agreement between the behavior predicted by the rate equations and the experimental findings, and in particular – the behavior in parallel magnetic field, provides a strong support for the validity of the model.

This work is supported by the Israeli Science Foundation, Grant No. 2139/20, and by the Minerva foundation.

## References

1. L. V. Keldysh, A. N. Kozlov, *Sov. Phys. JETP* **27**, 521 (1968).
2. “Bose-Einstein Condensation of Excitons and Biexcitons”, by S. A. Moskalenko and D. W. Snoke, Cambridge University Press (2000)
3. Yu E Lozovik and V I Yudson, *JETP Lett.* **22** 274 (1975)
4. D.W. Snoke, Coherence and optical emission from bilayer exciton condensates, *Adv. Condens. Matter Phys.* 938609 (2011).
5. M. Combescot, R. Combescot, and F. Dubin, *Rep. Prog. Phys.* **80**, 066501 (2017).
6. Yu.E. Lozovik , I.L. Kurbakov , G.E. Astrakharchik , J. Boronat , and Magnus Willander, *Solid State Commun.* **144**, 399 (2007).
7. A.V. Gorbunov and V.B. Timofeev, *JETP Lett.* **84**, 329 (2006).
8. A.A. High, J.R. Leonard, A.T. Hammack, M.M. Fogler, L.V. Butov, A.V. Kavokin, K.L. Campman, and A. C. Gossard, *Nature* **483**, 584 (2012).
9. Y. Shilo, K. Cohen, B. Laikhtman, K. West, L. Pfeiffer, and R. Rapaport, *Nat. Commun.* **4**, 2335 (2013).
10. M. Stern, V. Umansky, and I. Bar-Joseph, *Science* **343**, 55 (2014).
11. M. Alloing, M. Beian, M. Lewenstein, D. Fuster, Y. Gonzalez, L. Gonzalez, R. Combescot, M. Combescot, and F. Dubin, *EPL* **107**, 10012 (2014).
12. K. Cohen, Y. Shilo, K. West, L. Pfeiffer, and R. Rapaport, *Nano Lett.* **16**, 3726 (2016).
13. R. Anankine, M. Beian, S. Dang, M. Alloing, E. Cambril, K. Merghem, C. Gomez Carbonell, A. Lemaître, and F. Dubin, *Phys. Rev. Lett.* **118**, 127402 (2017)
14. S. Misra, M. Stern, A. Joshua, V. Umansky and I. Bar Joseph, *Phys. Rev. Lett.* **120**, 047402 (2018)
15. S. Dang, R. Anankine, C. Gomez, A. Lemaître, M. Holzmann, and F. Dubin, *Phys. Rev. Lett.* **122** 117402 (2019).
16. Z. Wang , D. A. Rhodes, K. Watanabe, T. Taniguchi, J. C. Hone , J. Shan, and K. F. Mak, *Nature* **574** 76 (2019).
17. M. Combescot, O. Betbeder-Matibet, R. Combescot, *Phys. Rev. Lett.* **99** 176403 (2007).
18. R. Combescot, M. Combescot, *Phys. Rev. Lett.* **109**, 026401 (2012).

19. B. Laikhtman and R. Rapaport, Phys. Rev. B **80**, 195313 (2009).
20. Y. Mazuz-Harpaz, K. Cohen, M. Leveson, K. West, L. Pfeiffer, M. Khodas, and Ronen Rapaport, PNAS **116** 18328 (2019).
21. Z. Vörös, R. Balili, D. W. Snoke, L. Pfeiffer, and K. West, Phys. Rev. Lett. **94**, 226401 (2005).
22. We find that the constant  $\Delta E$  extends a few hundreds  $\mu\text{m}$  further into the leads to the mesa.
23. See Supplementary Information.
24. D. Jaksch, C.W. Gardiner, K.M. Gheri and P. Zoller, Phys. Rev. A **58**, 1450 (1998)
25. I. Carusotto and C. Ciuti, Rev. Mod. Phys. **85**, 299 (2013).
26. J.R Leonard, Y.Y Kuznetsova, S. Yang, L.V Butov, T. Ostatnicky, A. Kavokin, and A.C Gossard, Nano Lett. **9**, 4204 (2009).
27. Spin Physics in Semiconductors, M. I. Dyakonov editor, Springer Series on Solid State Physics 157, ISSN 0171-1873.
28. R. Zimmermann, C. Schindler, Solid State Commun. **144**, 395 (2007).
29. L. V. Butov, A. V. Mintsev, Yu. E. Lozovik, K. L. Campman, and A. C. Gossard, Phys. Rev. B **62**, 1548 (2000).
30. In a Faraday configuration we observe a simple monotonous diamagnetic blueshift with no dip.
31. The PL intensity drops with  $B_{||}$ : The long lifetime allows the bright excitons to diffuse to the edges and recombine there. We therefore obtain  $n_1$  through the relation  $n_1 = I/\gamma_r$ .
32. G. Bastard, Phys. Rev B **46**, 4253 (1992).

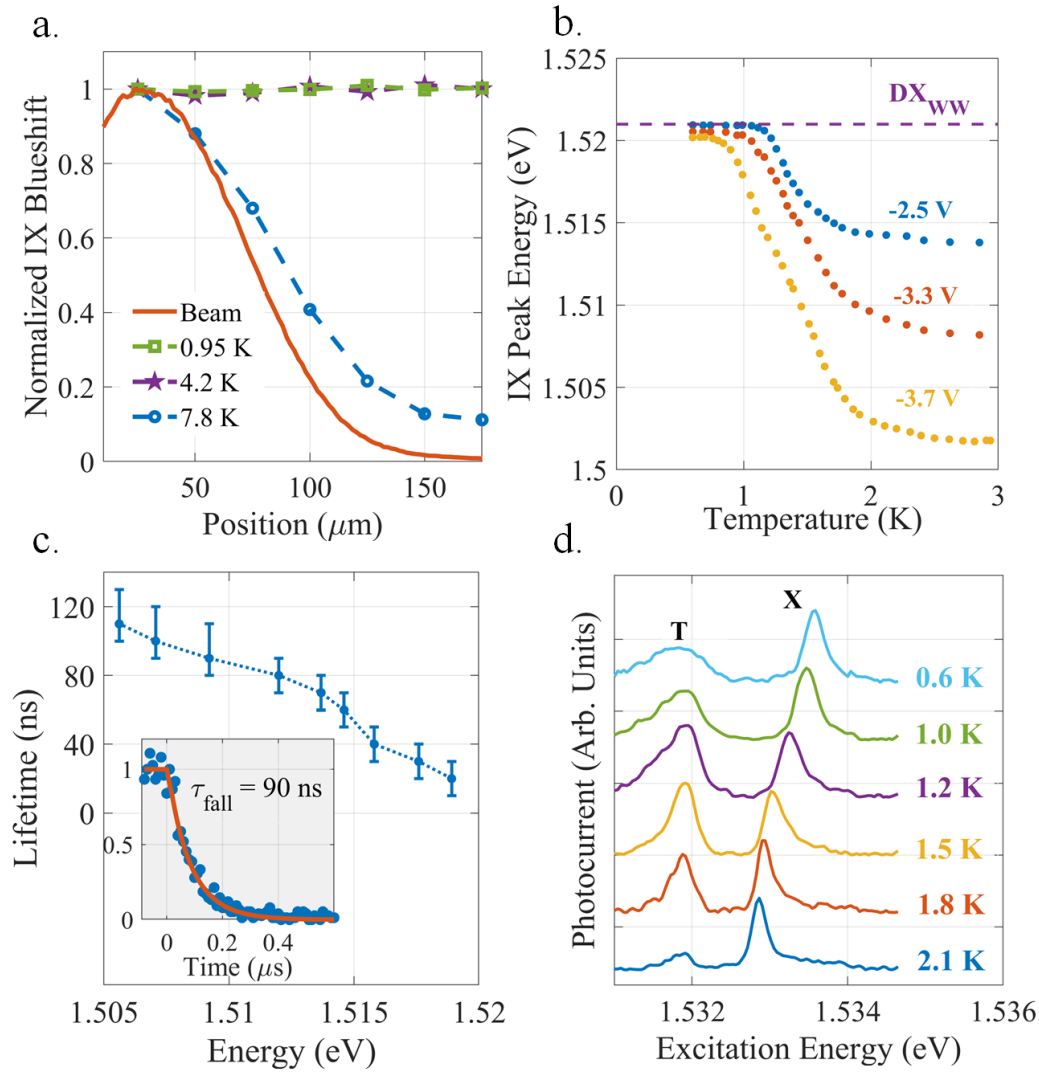


Figure 1: a. The IX blueshift along a horizontal cross-section of the mesa at three temperatures, normalized by its value at the center of the excitation beam. (The excitation beam profile is shown by the red solid line.) The transition to a constant blueshift at low temperatures can be clearly observed; b. The IX peak energy as a function of temperature at three gate voltages and a fix power  $P = 10 \mu\text{W}$ . The dashed line marks the energy of the wide-well exciton  $X_{\text{WW}}$ . c. The IX radiative lifetime as a function of peak energy. (inset) An exemplary trace of the lifetime measurement (blue data points) using correlated photon counting. The red line is a fit to exponential decay, with a fall time of 90 ns. d. Photocurrent spectra as the illuminating laser energy is tuned around the narrow-well exciton resonance at various temperatures in the range  $0.6 \text{ K} \leq T \leq 2.1 \text{ K}$ . Here  $V_g = -3.3 \text{ V}$  and  $P = 2 \mu\text{W}$ . The shift of the exciton peak, X, to higher energies and the broadening of the trion line, T, with decreasing temperatures are clearly seen.

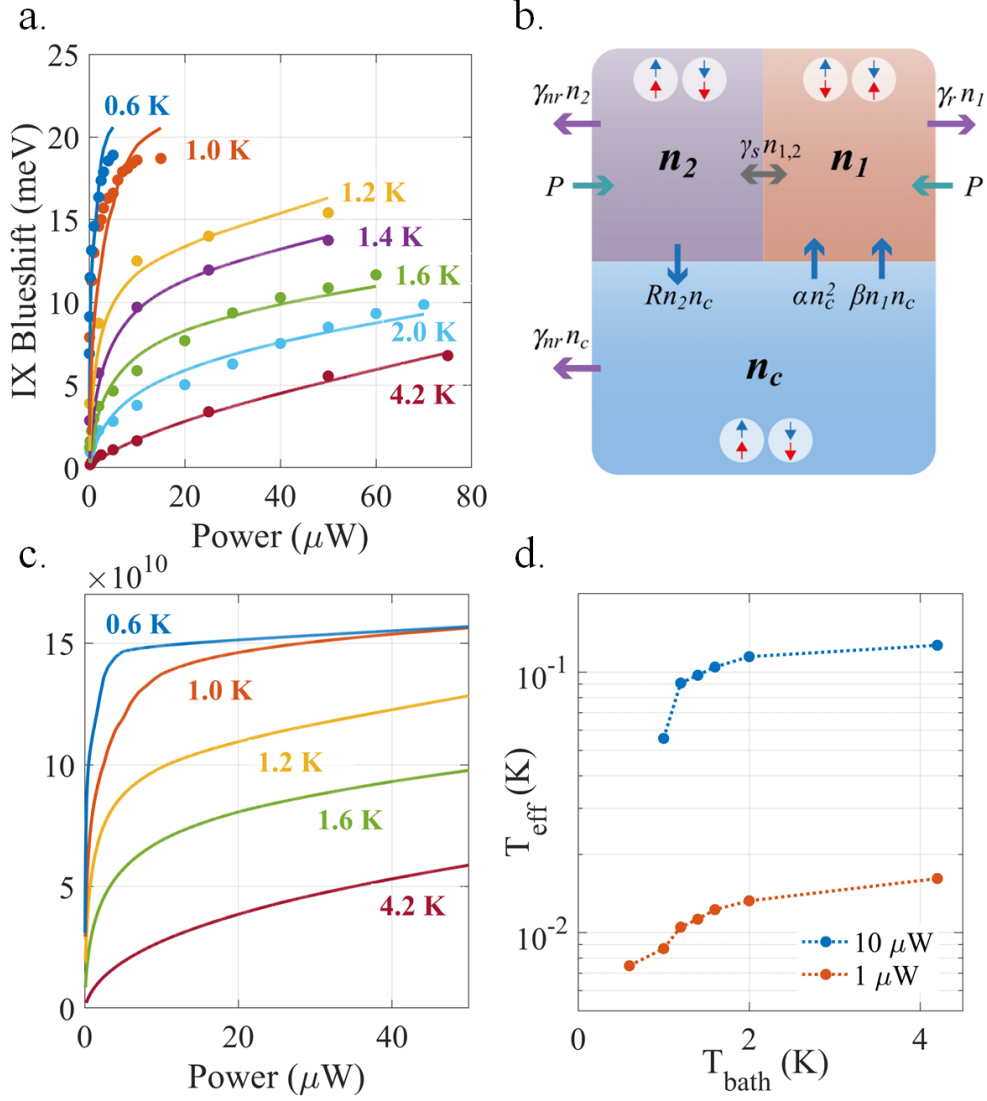


Figure 2: a. Filled circles - the measured power dependence of the IX blueshift  $\Delta E$  at various temperatures in the range 0.6K - 4.2K at  $V_g = -3.7\text{V}$ . The maximal  $\Delta E = 18\text{meV}$  is limited by the crossing of the  $X_{\text{WW}}$  line (See Fig. 1b). Solid lines - the steady-state solutions of the rate equations model. b. Schematic representation of the pumping, decay and particles exchange among the three reservoirs,  $n_1$ ,  $n_2$ , and  $n_c$ . The possible spin orientations of the electron and hole within the excitons are marked by the blue and red arrows, respectively. c. The calculated steady-state total exciton density. The temperatures are the same as in (a). d. The effective temperature as a function of the bath temperature at  $P = 1$  and  $10 \mu\text{W}$ . It is seen that  $T_{\text{eff}} \ll T_{\text{bath}}$  throughout, demonstrating the evaporative cooling of the system.

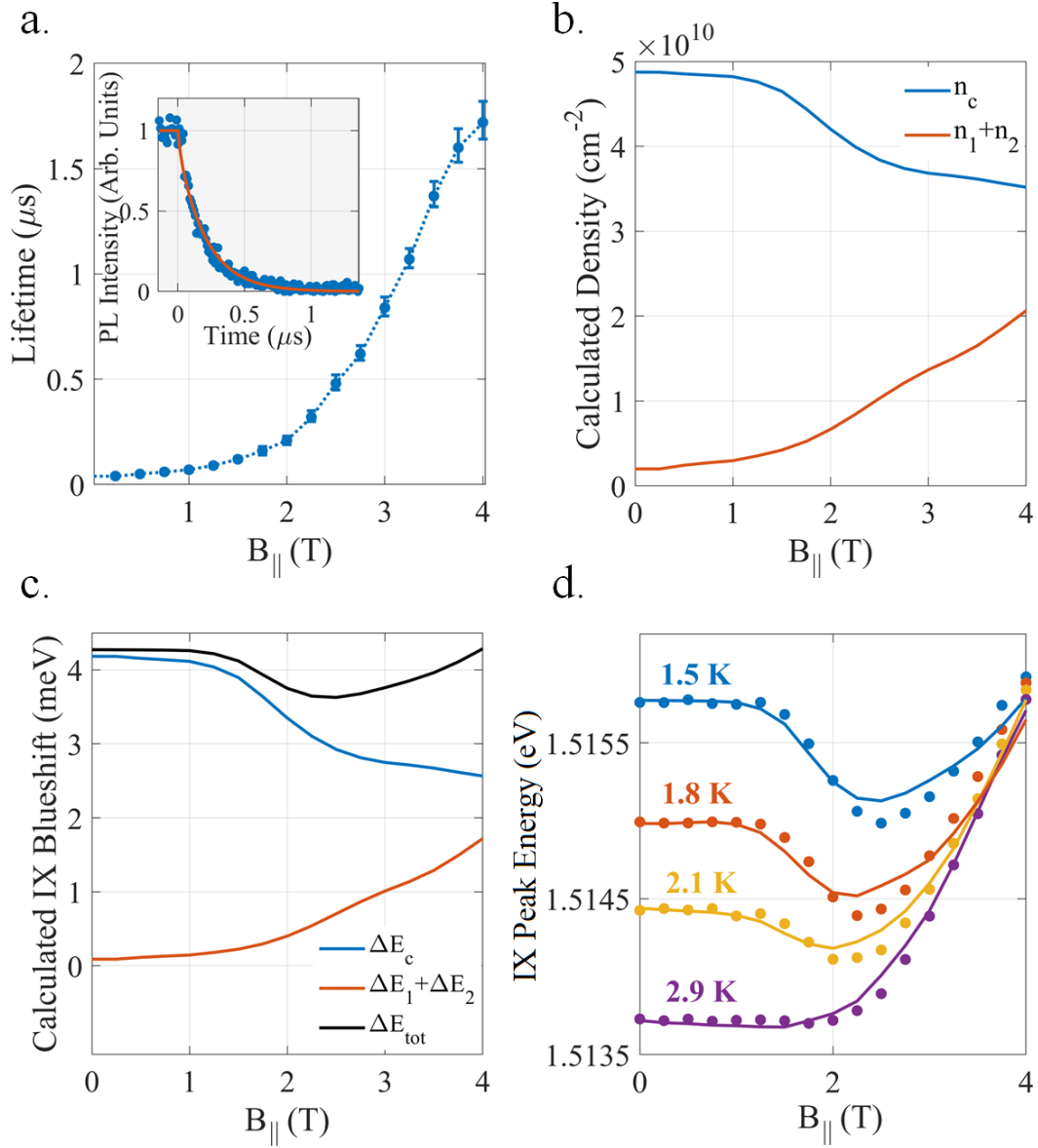


Figure 3: *a.* Measured radiative lifetime as a function of in-plane magnetic field at  $V_g = -2.5$  V,  $T = 1.5$  K and  $P = 10 \mu\text{W}$ . (inset) An example of a time-resolved measurement data (dots) at 2T and a fit to exponential decay (solid line); *b.* The calculated  $B_{\parallel}$ -dependence of density of the condensate,  $n_c$ , and the thermal part,  $n_1 + n_2$ . The depletion of  $n_c$  is clearly observed; *c.* The blueshift due to the condensate,  $\Delta E_c$ , and the thermal part,  $\Delta E_1 + \Delta E_2$ , as a function of  $B_{\parallel}$ , and the total blueshift,  $\Delta E_{\text{tot}} = \Delta E_c + \Delta E_1 + \Delta E_2$ . *d.* Dots - measured  $\Delta E$  as a function of  $B_{\parallel}$  at several temperatures. Solid lines - the corresponding calculated behavior.

# Formation Dynamics and Evaporative Cooling of a Dark Exciton Condensate: Supplementary Material

Subhradeep Misra<sup>1</sup>, Michael Stern<sup>2</sup>, Vladimir Umansky<sup>1</sup> and Israel Bar-Joseph<sup>1</sup>

<sup>1</sup>*Department of Condensed Matter physics, Weizmann Institute of Science, Rehovot, Israel*

<sup>2</sup>*Department of Physics, Bar-Ilan University, Ramat-Gan, Israel*

## Table of Contents

<b>I.</b>	<b>Materials and Methods</b> .....	2
<b>a.</b>	<b>Sample Structure</b> .....	2
<b>b.</b>	<b>Experimental Methods</b> .....	3
<b>c.</b>	<b>The Nonradiative Recombination</b> .....	3
<b>II.</b>	<b>The Rate Equations Model</b> .....	4
<b>III.</b>	<b>Approximated Solutions</b> .....	6
<b>a.</b>	<b>The Condensate at Zero Magnetic Field</b> .....	6
<b>b.</b>	<b>The Condensate Depletion in a Parallel Magnetic Field</b> .....	7
<b>IV.</b>	<b>Discussion of the model's parameters</b> .....	8
<b>a.</b>	<b>The value of <math>\alpha_0</math></b> .....	8
<b>b.</b>	<b>The correlation factor <math>f_{th}</math></b> .....	8
<b>c.</b>	<b>The value of <math>\beta</math></b> .....	8
<b>V.</b>	<b>Spin Relaxation of Dipolar Excitons</b> .....	9
<b>VI.</b>	<b>Extended Results</b> .....	10
	<b>References</b> .....	14

## I. Materials and Methods

### a. Sample Structure

The sample structure is nominally identical to that used in our previous works [1] and [2]. Namely, we have a coupled quantum well (CQW) system consisting of two GaAs wells having widths of 12 and 18 nm, respectively. These wells are separated by an  $\text{Al}_{0.28}\text{Ga}_{0.72}\text{As}$  barrier of thickness 3 nm. This system is embedded in a  $2\ \mu\text{m}$  thick  $n^+ - i - n^+$  structure having top and bottom silicon doped  $n^+$  layers of  $\text{Al}_{0.12}\text{Ga}_{0.88}\text{As}$  ( $n \sim 10^{18}\ \text{cm}^{-3}$ ), that allows application of a voltage perpendicular to the growth direction (Fig. S1a). The different well width allows us to conduct spectroscopic measurements in each well (see for example Fig. 1d of the manuscript). The dipole length,  $d$ , can be determined by taking the distance between the centers of the two wells,  $d = 18\ \text{nm}$ . The sample was processed using optical lithography, isotropic wet etching and metal deposition technique in order to form rectangular mesas of dimension  $200 \times 100\ \mu\text{m}^2$  (Fig. S1b).

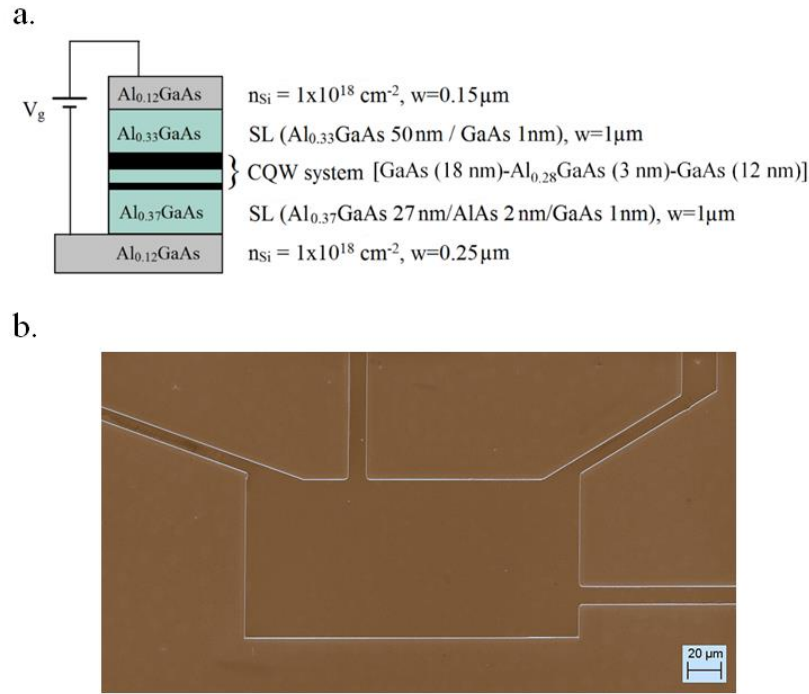


Figure S1: a. Schematic drawing of the sample structure (not to scale); b. Scanning electron micrograph (SEM) image of the mesa, where four connections to the top Ohmic contacts can be seen.



## **b. Experimental Methods**

The experiments are conducted in a dilution refrigerator with optical windows ( $0.05 < T < 6$  K), a variable temperature pumped helium cryostat ( $1.5 < T$ ) and a variable temperature 8T split-coil magneto-optic cryostat ( $1.5 < T$ ). This allowed us to cover the temperature and magnetic field range of interest for this work,  $0.1 < T < 10$  K and  $0 < B < 4$  T. For most of the experiments, a Gaussian beam with a  $60 \mu\text{m}$  radius (half width at half maximum) of a continuous wave laser at an energy  $1.590$  eV illuminates the sample. This energy is well below the barrier height, ensuring carriers are excited in the wells only, and carrier depletion effects are avoided [3]. The dark current through the sample at the relevant voltage range is  $\sim 100$  pA, and the photocurrent at the highest excitation power,  $100 \mu\text{W}$ , is below  $1$  nA.

The photoluminescence (PL) from the sample is guided to a U-1000 Jobin-Yvon Raman spectrometer to collect the spectra and analyze it, and is imaged on a cooled EMCCD camera (Andor iXon Ultra) with a spatial resolution of  $3 \mu\text{m}$ .

Spatially resolved spectroscopic measurements are performed using a pinhole having diameter  $20 \mu\text{m}$  placed at the focal plane of the collection objective. This allows selective collection of emitted light from various distinct areas of the mesa for imaging and spectroscopic analyses.

We carry out time-resolved measurements to determine the lifetime of indirect excitons (IX) using correlated photon counting system. To pulse the CW laser we use an acousto-optic modulator (AOM) with a rise time of  $17$  ns, and an Avalanche Photo-Diode (APD) is used to detect the photon events. The pulses to the AOM and the measurement time windows at the APD are synchronized by a fast arbitrary waveform generator (Tabor AWG WX1284) and a National Instruments Data Acquisition card (NIDAQ) is used for counting the APD output. A typical measured data is shown in the inset of Fig. 3(a) (filled circles), where the photon events are counted with a time resolution  $10\text{ns}$ . To extract the fall time ( $\tau$ ), we fit the data with an exponential decay,  $I = I_0 \exp\left(-\frac{t}{\tau}\right)$ . The resulting fitted curve is shown as the solid red line in that figure.

## **c. The Nonradiative Recombination**

We show in the following that the main contribution to the nonradiative recombination of the IX is the photocurrent:

- The number of e-h pairs that are generated at steady state at  $P = 10 \mu\text{W}$  illumination can be calculated as follows: We take the absorption coefficient,  $\kappa$ , at the excitation energy  $h\nu = 1.59 \text{ eV}$  as  $\kappa = 1.5 \times 10^4 \text{ cm}^{-1}$  [4], the absorption length  $L = 12 + 18 \text{ nm} = 30 \text{ nm}$ , and the transmission through the air-GaAs interface,  $T = 75\%$ . Hence, the number of pairs that are generated per second is:

$$N_{eh} \approx P \times \kappa \times L \times T \times \frac{1}{h\nu} =$$

$$= \frac{10^{-5} \times 1.5 \times 10^4 \times 30 \times 10^{-7} \times 0.75}{1.59 \times 1.602 \times 10^{-19}} = 1.3 \times 10^{12}$$

- The photocurrent at this power is  $\sim 100 \text{ pA}$ . Hence, the number of electrons that are removed from the system by the photocurrent in a second is:

$$N_{pc} = 10^{-10} / 1.602 \times 10^{-19} = 6.25 \times 10^8$$

- The ratio between the two is

$$R_1 = \frac{N_{pc}}{N_{eh}} \approx 5 \times 10^{-4}$$

- The measured radiative time is  $\sim 100 \text{ ns}$ , implying a radiative rate of  $\gamma_r \approx 10^7 \text{ s}^{-1}$ . The estimated nonradiative rate is  $\gamma_{nr} \approx 3 \times 10^3 \text{ s}^{-1}$ . Hence their ratio is

$$R_2 = \frac{\gamma_{nr}}{\gamma_r} \approx 3 \times 10^{-4}$$

We can see that  $R_1 \approx R_2$  implying that the dominant nonradiative channel is photocurrent.

We note, however, that spatial diffusion and recombination at the edges of the mesa reduces the PL intensity from the mesa. This effect is manifested as strong PL signal at the edges.

## II. The Rate Equations Model

Here we describe the rate equations model used to explain the temperature and magnetic field dependent IX energy shift. As mentioned in the text, at steady state we can classify the excitons in the system into two groups based on spin:  $J_z = \pm 1$  that can recombine radiatively and  $J_z = \pm 2$  that cannot couple to light due to angular momentum conservation law and may only recombine through slow non-radiative processes. Since only  $J_z = \pm 2$  states can condense, we assume these

excitons to be either thermal or condensed, whereas the  $J_z = \pm 1$  excitons are thermal only. Hence, we have three reservoirs in the system: thermal  $J_z = \pm 1$  excitons (with density  $n_1$ ), thermal long-lived  $J_z = \pm 2$  excitons ( $n_2$ ) and condensed  $J_z = \pm 2$  excitons ( $n_c$ ). The particles exchange among the three reservoirs and with the environment are schematically depicted in Fig. 2a of the manuscript and discussed in the main text. These considerations lead to the following system of equations:

$$\frac{\partial n_1}{\partial t} = P - \gamma_r n_1 - \gamma_s n_1 + \gamma_s n_2 + \alpha n_c^2 + \beta (n_1 + n_2) n_c \quad (1)$$

$$\frac{\partial n_2}{\partial t} = P - R n_2 n_c - \gamma_{nr} n_2 - \gamma_s n_2 + \gamma_s n_1 \quad (2)$$

$$\frac{\partial n_c}{\partial t} = R n_2 n_c - \alpha n_c^2 - \beta (n_1 + n_2) n_c - \gamma_{nr} n_c \quad (3)$$

Here  $P$  is the pumping power,  $\gamma_r$  and  $\gamma_{nr}$  are the radiative and non-radiative decay rate of the excitons, and  $\gamma_s$  is the spontaneous spin flip rate between  $n_1$  and  $n_2$ .  $R$  is the stimulated scattering rate from  $n_2$  to  $n_c$  [4],  $\alpha$  is the two particle scattering rate, and  $\beta$  is the scattering rate of  $n_c$  to  $n_1$  due to the rapid recombination of the dipolar bright excitons.

An important assumption here is that a condensate exciton cannot flip its spin spontaneously (at a rate  $\gamma_s n_c$ ), but can only do that through scattering with another condensate exciton (at a rate  $\alpha n_c^2$ ) or with a thermal exciton (at a rate  $\beta n_1 n_c$ ). We elaborate on this in section V below. Note that in the equations above we do not consider the spatial dependence of the various densities. Clearly, the spatial dependence of  $n_1$  and  $n_c$  is very different: While  $n_1$  should follow approximately the excitation beam profile,  $n_c$  is found to be constant throughout the mesa. We have repeated the measurements using a broad excitation beam, which is almost uniform across the mesa, and obtained very similar results. In fact, we find that the measured blueshift depends on the total power and is insensitive to the excitation beam profile. We can therefore conclude that this difference between the spatial profiles does not play an important role.

Figure S2 shows the calculated power dependence of the steady state densities  $n_1$ ,  $n_2$  and  $n_c$  at three temperatures, 4.2 K, 1.4 K and 1 K (note the different scales). The sublinear dependence of the condensate density is clearly observed at all temperatures.

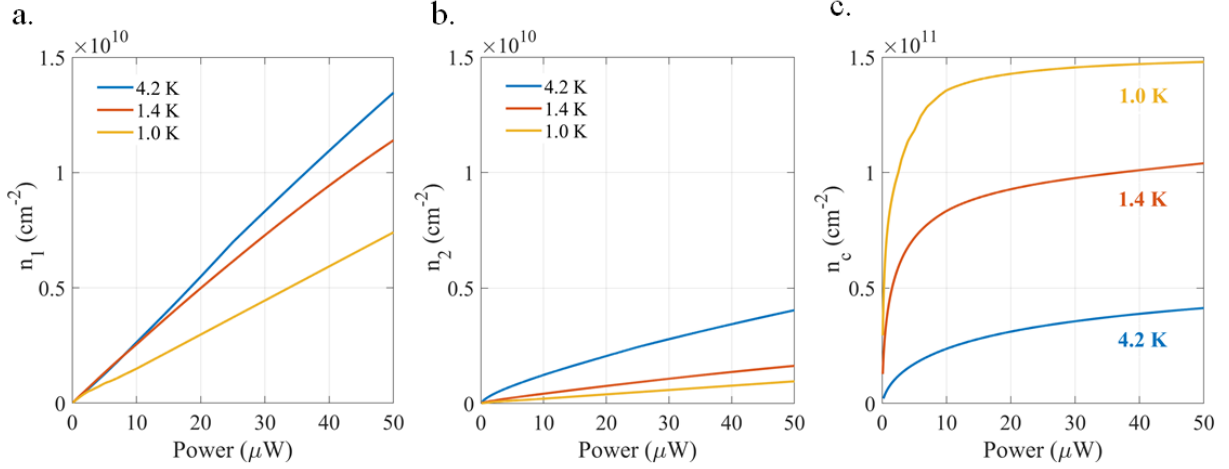


Figure S2: a-c. Excitation power dependence of the calculated densities of the individual reservoirs ( $n_1$  (a),  $n_2$  (b) and  $n_c$  (c)) at three different temperatures. The values of  $R, \alpha_0, \beta$  and  $T_0$  are taken from best fit to the data.

### III. Approximated Solutions

#### a. The Condensate at Zero Magnetic Field

The numerical solution of the equations for the total density  $n$  and blueshift  $\Delta E$  is given in the main text. Here we shall make a few approximations that simplify the expressions significantly and provide a physical intuition.

Firstly, we neglect processes governed by rate  $\gamma_{nr}$ , since their contribution is very small. We further neglect the spin relaxation processes,  $\gamma_s n_{1,2}$ , which at low temperatures are expected to be slower than  $\gamma_r$ . With these assumptions, summing the three equations at the steady state yields

$$0 = 2P - \gamma_r n_1$$

$$\Rightarrow n_1 = \frac{2P}{\gamma_r}$$

Also, from Eq. (2), we have,

$$P = R n_2 n_c$$

Plugging these values in Eq. (3), we get a quadratic equation for  $n_c$ :

$$\alpha n_c^2 + \beta \frac{2P}{\gamma_r} n_c + P \left( \frac{\beta}{R} - 1 \right) = 0 \quad (4)$$

The positive solution to this equation is

$$n_c = \frac{P\beta}{\alpha\gamma_r} \left[ \left( 1 + \frac{\alpha\gamma_r^2}{P\beta} \left[ \frac{1}{\beta} - \frac{1}{R} \right] \right)^{1/2} - 1 \right] \quad (5)$$

We can take now two limits:

- i.  $P \ll \frac{\alpha\gamma_r^2}{\beta} \left[ \frac{1}{\beta} - \frac{1}{R} \right]$ : This is the limit of low power or high temperatures ( $T > T_0$ ). We can approximate  $n_c$  as

$$n_c \approx \sqrt{\frac{\beta}{\alpha} \left[ \frac{1}{\beta} - \frac{1}{R} \right] P} = C_1(\alpha, \beta, R) \sqrt{P} \quad (6)$$

We can see that at this limit  $n_c$  exhibits a sublinear power dependence of  $\sqrt{P}$ .

- ii.  $P \gg \frac{\alpha\gamma_r^2}{\beta} \left[ \frac{1}{\beta} - \frac{1}{R} \right]$ : This is the limit of high power or low temperatures, ( $T \ll T_0$ ). The expression for  $n_c$  becomes

$$n_c \approx \left[ \frac{1}{\beta} - \frac{1}{R} \right] \frac{\gamma_r}{2} = C_2(\gamma_r, \beta, R) \quad (7)$$

We can see that at this limit  $n_c$  becomes independent of power. This yields the saturated behavior of the IX energy shift with  $P$ .

### **b. The Condensate Depletion in a Parallel Magnetic Field**

The behavior of the condensate density ( $n_c$ ) as a function of in-plane magnetic field ( $B_{\parallel}$ ) can also be visualized from the approximate expression. It has been shown in the main text that  $B_{\parallel}$  essentially shifts the dispersion in momentum space and modifies the radiative decay rate,  $\gamma_r$ . Hence, we can take again here two limits, of large and small  $\gamma_r$ .

- i. At  $B_{\parallel}=0$ , where  $\gamma_r$  is large and the power is low, we are in the limit  $\gamma_r^2 \gg \frac{P\beta}{\alpha} / \left[ \frac{1}{\beta} - \frac{1}{R} \right]$ . This is identical to the low power limit, and  $n_c$  is independent of  $\gamma_r$  (see Eq. (6)).

At high  $B_{\parallel}$ , when  $\gamma_r$  becomes very small (Fig. 3a), we are in the limit  $\gamma_r^2 \ll \frac{P\beta}{\alpha} / \left[ \frac{1}{\beta} - \frac{1}{R} \right]$ . This is identical to the high  $P$  limit discussed earlier, which yields  $n_c \approx \gamma_r/2\beta$ . At this limit the condensate density is depleted with decreasing  $\gamma_r$ .

## IV. Discussion of the model's parameters

### a. The value of $\alpha_0$

For the calculation of  $\alpha_0$  we use the derivation of the exchange integral  $\xi$  of Ref. 6. From Fig. 1 of that work it follows that  $|\xi|/(R_X a_X^2) = 3 \times 10^{-4}$ , where  $R_X$  is the exciton binding energy and  $a_X$  is the exciton radius (Note that we used here the exchange integral density rather than the integral itself used in the expression of Ref. 6. Taking  $R_X = 2\text{meV}$ ,  $a_X = 10\text{ nm}$  we get that  $\alpha_0 = \frac{|\xi|}{h} = \frac{3 \times 10^{-4} \times 2 \times 1.6 \times 10^{-22} \times 10^{-16}}{6.6 \times 10^{-34}} \approx 1.5 \times 10^{-8} \text{ m}^2\text{s}^{-1}$ . This value is in an excellent agreement with the value obtained from the fit!

### b. The correlation factor $f_{th}$

The correlation factor,  $f_{th}$ , in Eq. (2) of the manuscript depends on density and temperature, and originates from the repulsive interaction among the excitons, which prevents them from coming arbitrary close to each other [7-9]. For the density dependence of  $f_{th}$  we used the calculated screened exciton-exciton interaction curve [Fig. 1 of Ref. 9], and the temperature dependence is taken from the low density expression  $f_{th}(T) = \Gamma\left(\frac{4}{3}\right) \left(\frac{4\pi\epsilon d T}{8e^2}\right)^{1/3}$  [8], where  $\epsilon$  is the dielectric constant of the medium,  $d$  is the mean electron-hole separation, and  $e$  is the charge of an electron. Figure S3a shows the calculated value of  $f_{th}$  as a function of density for  $T = 4.2\text{ K}$ ,  $2.0\text{ K}$  and  $1.0\text{ K}$ .

### c. The value of $\beta$

Figure S3b shows the value of  $\beta$  that is obtained from the fit. It can be seen that it exhibits a weak temperature dependence, varying by  $\sim 30\%$  over the whole range. To get an insight into the value of  $\beta$ , which is a scattering related spin flip rate, let us express it as  $\beta \approx a^2 \gamma_s$ , where  $a$  is a scattering

length and  $\gamma_s$  is the spin flip rate. Taking  $\gamma_s^{-1} \approx 100$  ns [10], we obtain  $a \approx 40$  nm, approximately twice the exciton diameter.

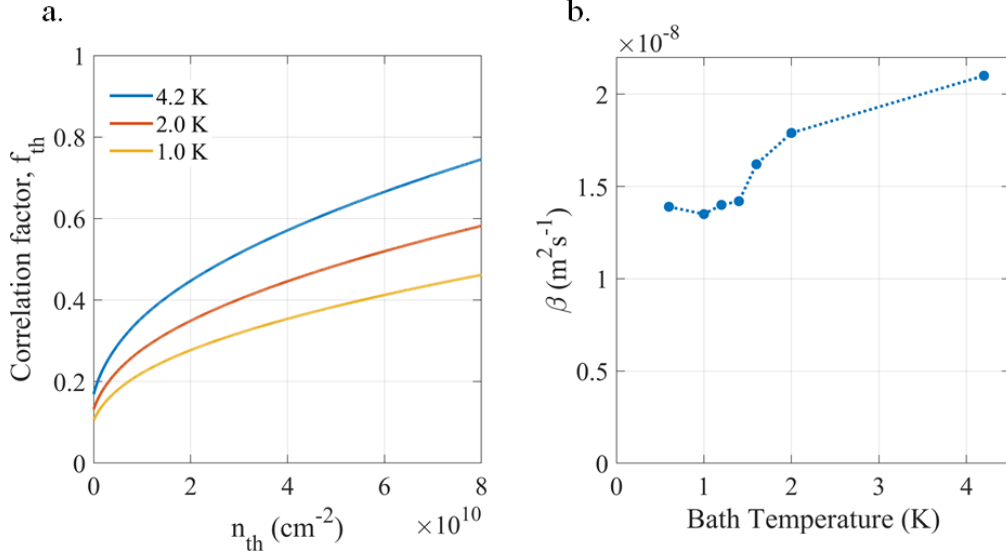


Figure S3: a. The correlation factor,  $f_{th}$ , as a function of the thermal part density ( $n_{th}$ ) at three different temperatures; b. The fitted parameter  $\beta$  as a function of bath temperature.

## V. Spin Relaxation of Dipolar Excitons

The relaxation time of the dipolar exciton spin in GaAs CQW is known to be much longer than the corresponding time in single quantum well (SQW) [10, 11]. The dominant process which determines the exciton spin relaxation time is the Dyakonov-Perel (DP) mechanism [12]. The DP mechanism originates from momentum scattering of the excitons. These scattering events change the precession axis of the exciton spin, around the random magnetic (and electric) fields they experience while moving in the non-centrosymmetric crystal. The discussion above applies for thermal exciton. However, for a condensate, which at mean field approximation can be considered to be at  $k = 0$ , momentum scattering is suppressed, and therefore, the DP mechanism is suppressed as well. Hence, one can neglect the spontaneous spin relaxation of the condensate excitons.

In the manuscript we took the field dependence of  $\beta$  to be  $\beta(B) = \beta(0)B^{-1/2}$ . Clearly, this  $B^{-1/2}$  dependence is not valid at arbitrary low magnetic field. As shown in Ref. 32 of the manuscript, the

validity criterion for the  $B^{-\frac{1}{2}}$  behavior is  $\hbar\omega_c \gg \Gamma$ , where  $\omega_c$  is the cyclotron frequency and  $\Gamma$  is the Landau level width. In our case, we take the validity range to be  $B > 1$  T, where  $\hbar\omega_c \approx 2$  meV and  $\Gamma \approx 1$  meV. Below this field,  $\beta$  is taken to be gradually changing to the zero magnetic field value.

## VI. Extended Results

Below we show representative spectra from which the data in the manuscript were extracted.

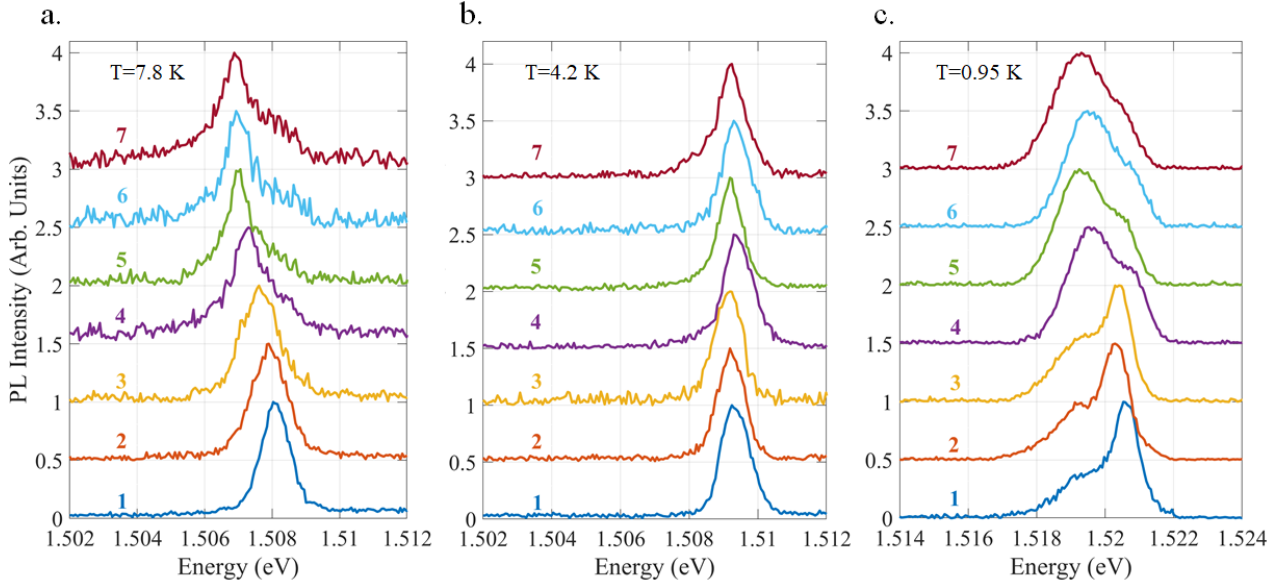


Figure S4: Normalized PL spectra measured as a function of position along the mesa at three different temperatures (a. 7.8 K, b. 4.2 K and c. 0.95 K). The spectra are vertically shifted for clarity. The peak position of these spectra are used to obtain Fig. 1a of the manuscript. The numbers denote the different locations from which the PL is collected: No. 1 corresponds to the leftmost data point of Fig. 1a and No. 7 - to the rightmost data point, hence one moves away from the excitation beam while proceeding from 1 to 7. In all the measurements,  $P = 10 \mu\text{W}$  and gate voltage is kept fixed at  $-3.3$  V. At the lowest temperature,  $T = 0.95$  K, the IX comprises of two peaks, which change oscillator strength as one moves away from the excitation beam area. This change does not affect their peak position. The origin of this splitting is being studied and will be discussed elsewhere.



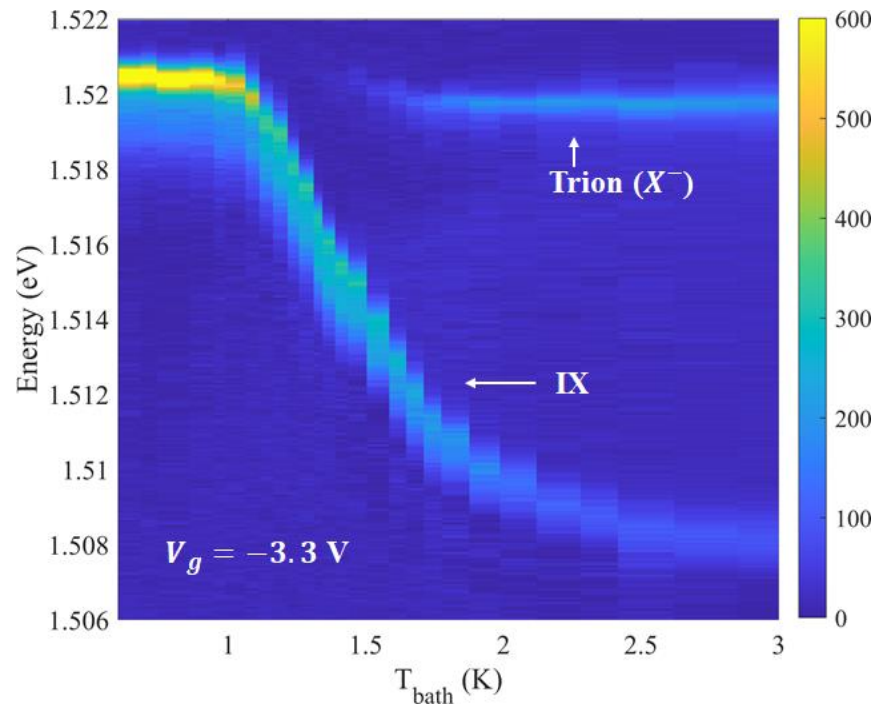


Figure S5: A compilation of PL spectra collected from the whole sample as a function of bath temperature, where the excitation beam is positioned centrally on the mesa. The color code denotes the PL intensity. Here  $P = 10 \mu\text{W}$  and gate voltage is kept fixed at  $-3.3 \text{ V}$ . The negatively charged trion ( $X^-$ ) of the wide well and the IX are labelled.

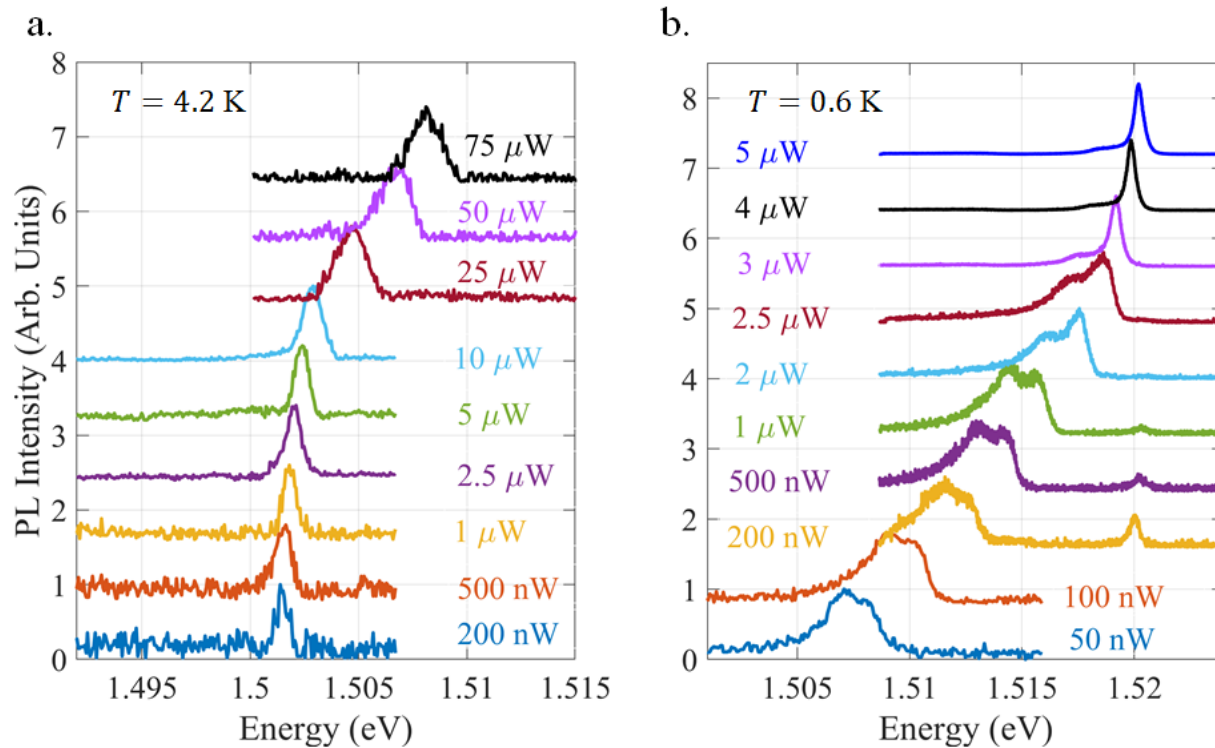


Figure S6: Power dependence of the normalized PL spectra at two different temperatures: a. 4.2 K; and b. 0.6 K. In both measurements, the gate voltage is kept fixed at  $-3.7$  V (Note the different energy scales). The sharp peak at the highest powers in b is due to the merging of the IX with the wide well exciton.

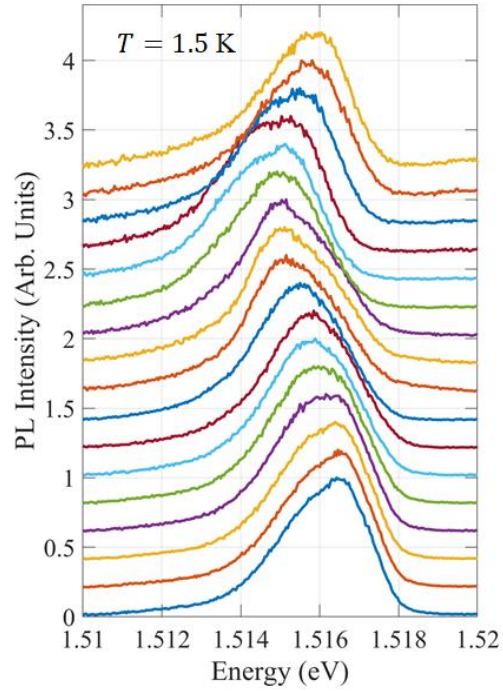


Figure S7: In-plane magnetic field ( $B_{||}$ ) dependence of the normalized PL spectra at bath temperature of 1.5 K. Here the excitation power is  $10 \mu\text{W}$  and the gate voltage is kept fixed at  $-2.5 \text{ V}$ . The spectra are taken in the range  $0 \text{ T} \leq B_{||} \leq 4 \text{ T}$ , with the spacing being  $0.25 \text{ T}$ . The bottom spectrum (blue) corresponds to  $B_{||} = 0 \text{ T}$ . The spectra are vertically shifted for clarity.

## References

1. M. Stern, V. Umansky, and I. Bar-Joseph, *Science* **343**, 55 (2014).
2. S. Misra, M. Stern, A. Joshua, V. Umansky and I. Bar Joseph, *Phys. Rev. Lett.* **120**, 047402 (2018).
3. R. Rapaport, Gang Chen, D. Snoke, Steven H. Simon, Loren Pfeiffer, Ken West, Y. Liu, and S. Denev, *Phys. Rev. Lett.* **92**, 117405 (2004).
4. W. T. Masselink, P. Pearah, J. Klem, C. Peng, H. Morkoç, G. Sanders, Y.-C. Chang, *Phys. Rev. B* **32**, 8027 (1985).
5. I. Carusotto and C. Ciuti, *Rev. Mod. Phys.* **85**, 299 (2013).
6. Y. Mazuz-Harpaz, K. Cohen, M. Leveson, K. West, L. Pfeiffer, M. Khodas, and R. Rapaport, *PNAS* **116**, 18328 (2019).
7. C. Schindler and R. Zimmermann, *Phys. Rev. B* **78**, 045313 (2008).
8. B Laikhtman and R. Rapaport, *Phys. Rev. B* **80**, 195313 (2009).
9. A. L. Ivanov, E. A. Muljarov, L. Mouchliadis, and R. Zimmermann, *Phys. Rev. Lett.* **104**, 179701 (2010).
10. K. Kowalik-Seidl, X. P. Vögele, B. N. Rimpfl, S. Manus, J. P. Kotthaus, D. Schuh, W. Wegscheider, and A. W. Holleitner, *Appl. Phys. Lett.* **97**, 011104 (2010).
11. J. R. Leonard, Y. Y. Kuznetsova, Sen Yang, L. V. Butov, T. Ostatnicky, A. Kavokin, and A. C. Gossard, *Nano Lett.* **9**, 4204 (2009).
12. *Spin Physics in Semiconductors*, M. I. Dyakonov editor, Springer Series on Solid State Physics **157**, ISSN 0171-1873.